Journal of Power Sources 230 (2013) 81–88

Contents lists available at SciVerse ScienceDirect

Journal of Power Sources

journal homepage: www.elsevier.com/locate/jpowsour

A facile preparation of novel Pt-decorated Ti electrode for methanol electro-oxidation by high-energy micro-arc cladding technique

Xiaoguang Wang [a,*], Zhonghua Zhang [b], Bin Tang [a], Naiming Lin [a], Huilin Hou [a], Yong Ma [a]

[a] Research Institute of Surface Engineering, Taiyuan University of Technology, Yingze West Road 79, Taiyuan 030024, PR China
[b] Key Laboratory for Liquid-Solid Structural Evolution and Processing of Materials (Ministry of Education), Shandong University, Jingshi Road 17923, Jinan 250061 PR China

HIGHLIGHTS

- Novel Pt/Ti electrode is prepared by high-energy micro-arc cladding technique.
- Pt/Ti electrode shows high catalytic activity and excellent anti-poisoning effect.
- Typical structural and chemical effects may be responsible for promising performance.

ARTICLE INFO

Article history:
Received 7 August 2012
Received in revised form
4 November 2012
Accepted 6 December 2012
Available online 13 December 2012

Keywords:
Methanol
Electrocatalysis
Micro-arc deposition
Anti-poisoning effect
Platinum–titanium

ABSTRACT

In this paper, a novel Pt-decorated Ti electrode was prepared by a high-energy micro-arc cladding (HEMAC) technique for methanol electro-oxidation in alkaline media. The surface structure, morphology, composition and electrocatalytic properties were investigated by thin-film X-ray diffraction (TF-XRD), scanning electron microscopy-energy dispersive X-ray analysis (SEM-EDX) and electrochemical measurements. The results show that the $Pt_{arc\text{-}dep}Ti$ surface mainly comprises Ti, Pt, Pt_3Ti and $PtTi_3$. Moreover, a coarsening topographical morphology can be obtained, being composed of numerous craters/spots with sizes ranging from nano-scales to several microns. The $Pt_{arc\text{-}dep}Ti$ alleviates the CO poisoning effect of methanol electro-oxidation with a higher ratio of the forward anodic peak current (I_f) to the reverse anodic peak current (I_b). The improvement in the catalytic performance should be attributed to that the surrounding Ti sites ameliorate the tolerance to CO adsorption on Pt islands. The $Pt_{arc\text{-}dep}Ti$ electrode reveals its superior electrocatalytic performance toward methanol oxidation and will find promising applications in fields of catalysis, fuel cells and so forth.

© 2012 Elsevier B.V. All rights reserved.

1. Introduction

Direct methanol fuel cell (DMFC) has attracted great attention in portable devices and transportation applications because of its high energy density, low cost, and easiness in transportation and storage [1–4]. At present, the Pt and PtRu are considered as the best electrocatalysts for the DMFCs, especially in acidic circumstance. However, the complete direct electro-oxidation of methanol is difficult to carry out due to strongly bound CO-like intermediate species in acid electrolytes. Unlike in acid, the electrode does not suffer severely from poisoning in alkali because the bonding of chemisorbed intermediates on Pt is weak and the amount of suggested poisoning species CO_{ads} is smaller than that in acidic media [5]. Several studies have also reported that methanol can be oxidized more efficiently in alkaline media as compared to that in acidic solution owing to the presence of an excess concentration of OH^- ions [6–8]. In addition, the alkaline media (i.e. KOH) is less aggressive/corrosive to metal or/and carbon than acid. And thus, the less-corrosive nature of an alkaline environment ensures a potential greater longevity and allows the implementation of non-noble catalysts (i.e. nickel and stainless steel), both for the cathode and the anode. Generally, the fuel cell equations for the direct use of methanol with an alkaline electrolyte are described below [9]:

Cathode: $4e^- + O_2 + 2H_2O \rightarrow 4OH^-$

Anode: $CH_3OH + 2OH^- \rightarrow HCHO + 2H_2O + 2e^-$ (Step 1)

$HCHO + 2OH^- \rightarrow HCOOH + H_2O + 2e^-$ (Step 2)

* Corresponding author. Tel./fax: +86 351 6010540.
E-mail addresses: wangxiaoguang@tyut.edu.cn, wangxiaog1982@163.com (X. Wang).

0378-7753/$ – see front matter © 2012 Elsevier B.V. All rights reserved.
http://dx.doi.org/10.1016/j.jpowsour.2012.12.026

$HCOOH + 2OH^- \rightarrow CO_2 + 2H_2O + 2e^-$ (Step 3)

However, one of the main issues operating DMFC in the alkaline electrolyte is that the CO_2 produced reacts with the electrolyte to form carbonate salts [10]. For example, when contacting with CO_2, KOH reacts to form potassium carbonate (K_2CO_3), thereby reducing the OH^- concentration. If a significant reduction in the concentration of OH^- ions occurs, one observes a reduction in the ionic-conductivity of the electrolyte as well as an increase of the electrolyte viscosity. Additionally, K_2CO_3 precipitates and may block gases pores and thus limit the gas diffusion inside the catalytic layer to the active sites. Fortunately, it should be noted that it is rarely to achieve such a high concentration of K_2CO_3 at a mild KOH bulk concentration (i.e. less than ~6 M) at common operating temperatures (20–70 °C) [11]. Moreover, precipitation can be avoided by ensuring a good circulation of the electrolyte as well as applying appropriate modification of the electrode pore structure [12].

In order to both reduce the usage of precious metals and increase the active sites, a variety of low-dimensional nanoparticles or films are generally synthesized as basic catalytic electrode units. Furthermore, alloying Pt with other transition metals M (such as Ni, Co, Fe, etc) not only reduces Pt loading, but also has a significant impact on Pt electrocatalytic performance owing to the intrinsic alloying effect [13,14]. In previous papers, however, the strategies for synthesis of Pt or Pt-based catalysts were mainly limited within several liquid-phase-involved routes in suitable chloroplatinate-containing solutions, such as electrochemical/electro-less deposition, hydrothermal reduction, and so forth [15–17].

Nowadays, the high-energy micro-arc cladding (HEMAC) or electro-spark deposition (ESD) process has gained increasing interest as a promising surface modification technique owing to its efficiency, simplicity and cost-effectiveness [18,19]. The HEMAC is essentially a surface pulsed-arc micro-welding process, in which periodic electric arcs are produced through a conductive source electrode (positive pole) energized by a series of capacitors as it is momentarily short-circuited with the base material (negative pole). During the arc generation (the duration is typically 1–10 μs with a maximum arc temperature reaching 5000–25,000 K [20]), the electrode material will be partially melted to form quantities of small liquid droplets. These droplets are accelerated through the arc, impact against the base metal substrate, solidified rapidly and build-up [21,22]. The main advantage associated with the HEMAC process is that the metallurgical bonded coatings with a strong adherent interface can be produced with little heat input to the substrate which remains at or near ambient temperature. In the past decades, however, such an efficient surface modification strategy merely aroused attention in the field of engineering materials (such as anti-wear coating deposition or repairing).

It was well-documented that Ti would be an ideal substrate for electrocatalytic electrode due to its low cost, superior mechanical strength and especially the intrinsic character prone to adsorb hydroxyl and oxygen-containing species [23,24]. Hassan [25] investigated the electrochemical activity of electrodeposited Pt and Pt–Sn nanoparticles on Ti as anodes for direct methanol fuel cells and reported that the combination effect of Pt, Sn and Ti improves the catalytic activity and stability through complete oxidation of intermediate products. Yi et al. [26] also fabricated a bimetallic nano-catalyst through co-deposition of Pt and Sn on a Ti surface using a one-step hydrothermal method, which exhibits a high electrocatalytic activity for the formic acid and methanol oxidation. Electro-oxidation of methanol was also studied on the Ti mesh coated with PtRu [27], the platinized Ti electrode [28] and finely dispersed Pt on Ti [29]. In all cases, these Ti-supported Pt and Pt-related catalysts reveal an enhanced catalytic activity.

In the present study, we synthesized a novel Pt-decorated Ti catalytic electrode using the HEMAC method. To our best of acknowledge, this is the first attempt to extend HEMAC for surface modification of catalytically active Ti-supported electrode. The physicochemical properties were examined by thin-film X-ray diffraction (TF-XRD), scanning electron microscopy (SEM) and energy dispersive X-ray analysis (EDX). The electrocatalytic activity for methanol oxidation was evaluated in an alkaline media by cyclic voltammetry (CV) and chronoamperometry (CA).

2. Experimental

2.1. Preparation

Disc-shaped pure Ti substrate (Φ14 × 2 mm, 99.95 wt.% purity) was mechanically polished, ultrasonically cleaned in acetone, alcohol and ultra-purified water, and then dried. The micro-arc deposition was conducted using a SQ-2 commercial electric spark alloying apparatus (Northwestern Polytechnical University, China [30]) with a commercially pure Pt rod (Φ1 × 20 mm, 99.9 wt.% purity) equipped on a hand-held gun as the source electrode. The deposition parameters were fixed at a voltage of 40 V and a capacitance of 600 μF in a controlled argon atmosphere at ambient temperature. Fig. 1 shows schematic diagrams of the principle working circuit of HEMAC apparatus and the sketch of Pt arc-depositing process. When the source electrode contacted on the substrate surface, micro-electric arc (spark) with high temperature was generated due to the occurrence of momentarily short-circuit, resulting in partial melting of both electrode materials. Then, the molten metals were mixed together and rapidly solidified to form a micro-crystalline spot region. This process was performed repeatedly until Pt arc-deposited throughout the whole surface of target Ti disk. After that, the $Pt_{arc\text{-}dep}Ti$ sample was rinsed using ultra-purified water and dehydrated alcohol.

2.2. Characterization

Phase identification of the $Pt_{arc\text{-}dep}Ti$ was performed on a thin-film X-ray diffractometer (TF-XRD, Shimadzu XRD-7000) with Cu Kα radiation ($\lambda = 1.5406$ Å). The top surface microstructure and chemical composition were characterized using a field emission scanning electron microscope (SEM, S-4800, Hitachi) and an energy dispersive X-ray (EDX) analyzer which was attached to SEM.

2.3. Electrochemical measurements

Electrochemical measurements were conducted using a CS-350 Potentiostat. The as-deposited $Pt_{arc\text{-}dep}Ti$, an Hg/HgO/KOH (1.0 M) (MMO) and a Pt plate were used as working, reference and counter electrode, respectively. Moreover, a bare Ti disk and a flat Pt sheet with an area of 1 cm^2 were also chosen as a reference to compare with the $Pt_{arc\text{-}dep}Ti$ sample. All potentials refer to MMO. If no special emphasis, the geometric surface area of the working electrode was used to normalize the current densities. Voltammetric behavior was characterized in a 0.5 M KOH solution de-aerated with N_2. The electrocatalytic activity measurements were carried out in 0.5 M KOH solution containing methanol with appropriate concentrations. All electrochemical experiments were performed at ambient temperature (~25 °C).

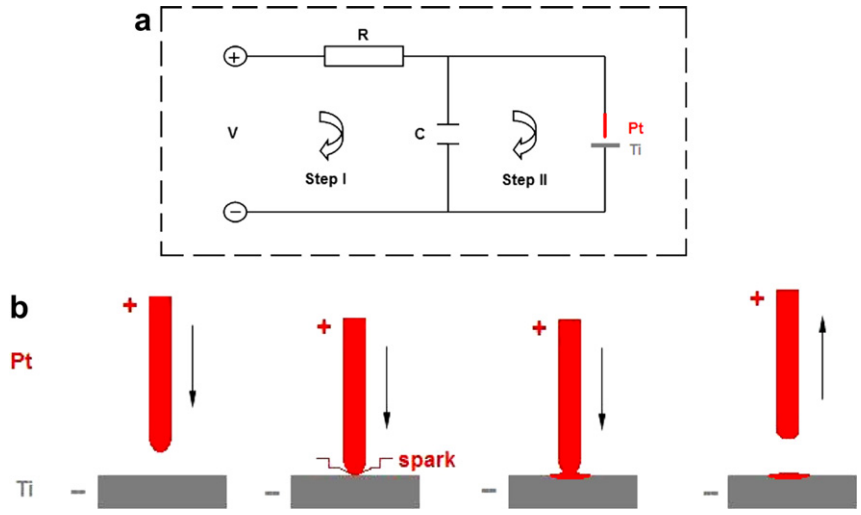

Fig. 1. Schematic diagram of Pt arc-deposited on Ti ($Pt_{arc\text{-}dep}Ti$) using the HEMAC technique. (a) Principle working circuit and (b) sketch of deposition process.

3. Results and discussion

3.1. Surface phase constitution, morphology and composition of the $Pt_{arc\text{-}dep}Ti$ sample

The basic principle of HEMAC and the arc deposition scheme of Pt on Ti were schematically illustrated in Fig. 1a and b. The details referring to this surface modification technique can be found elsewhere [19–22]. Fig. 2 shows the macroscopical surface feature of bare Ti substrate and arc-deposited $Pt_{arc\text{-}dep}Ti$ sample. Before deposition, the Ti disc depicted a smooth surface (Fig. 2a). After arc deposition of Pt, however, an evenly distributed Pt-related cladding layer with a rough appearance was obtained (Fig. 2b). It is observable that the $Pt_{arc\text{-}dep}Ti$ surface consists of countless fine spherical clusters with a pit-and-knap structure.

Fig. 3 shows surface XRD pattern of the $Pt_{arc\text{-}dep}Ti$ sample. Although some diffraction peaks merged together, several phases referring to Pt and Ti can be clearly identified. By comparing with standard lines, it indicates the surface of $Pt_{arc\text{-}dep}Ti$ mainly comprises Ti, Pt, Pt_3Ti and $PtTi_3$. Based upon the XRD result, it is reasonable to assume that during the arc-deposition process, the partial melting/alloying of Pt and Ti contributes to the formation of these Pt or Ti-involved intermetallic compounds (i.e. Pt_3Ti, $PtTi_3$, etc). Besides, some Pt droplets solidify quickly on the Ti surface to form Pt clusters (Pt phase) while the Ti signals should come from the substrate due to the micro-intervals between Pt clusters. .

Fig. 4 shows top-view SEM micrograph and corresponding EDX spectrum of the $Pt_{arc\text{-}dep}Ti$ sample. As shown in Fig. 4a, it is clear that the surface is composed of numerous craters/spots with sizes ranging from nano-scales to several microns. Typical fine and large craters/spots are marked by an upward and downward arrow, respectively. Normally, the micro-sparks that are continuously struck between the tip of Pt anode and the superficial layer of base Ti cause molten pools, which then solidify, with the associated shrinkage, to form craters. And the splash spots mainly derived from the impact of the accelerated molten Pt droplets by the plasma jet on the substrate at high velocity. Thus, the typical craters/spots appearance is the main feature of the HEMAC technique. At a higher magnification, some tiny cracks are visible on the surface and highlighted by arrows in Fig. 4b. Commonly, it is believed that tensile stress is the direct driving force of cracking [22]. Parkansky et al. [31] investigated the build-up of residual tensile stress during the HEMAC process and demonstrated that the predominant stress relief and surface damage mechanism is surface cracking. It is noteworthy that the residual stress in the HEMAC layer is always tensile, because the bulk of the substrate is cool, while the newly applied layer is “hot”. Therefore, the

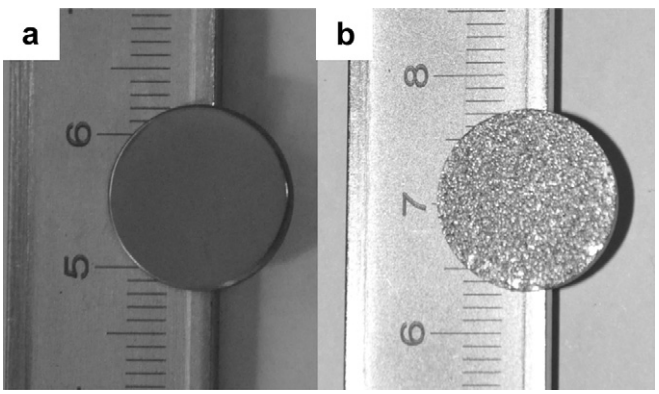

Fig. 2. Macrographs of (a) bare Ti substrate and (b) as-deposited $Pt_{arc\text{-}dep}Ti$ sample.

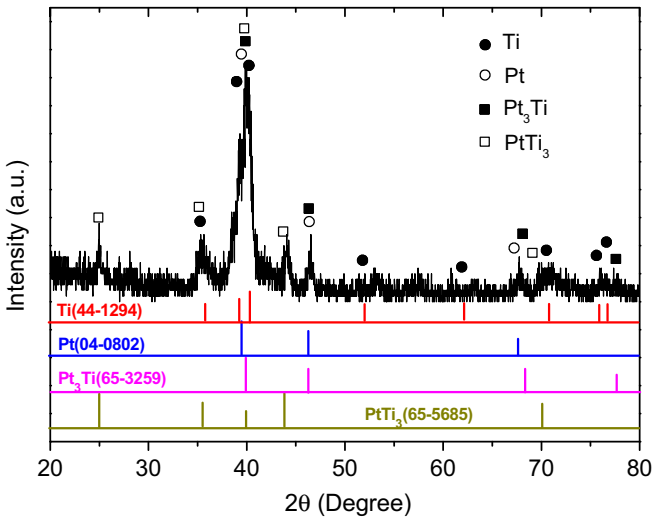

Fig. 3. Surface thin-film XRD pattern of $Pt_{arc\text{-}dep}Ti$ sample.

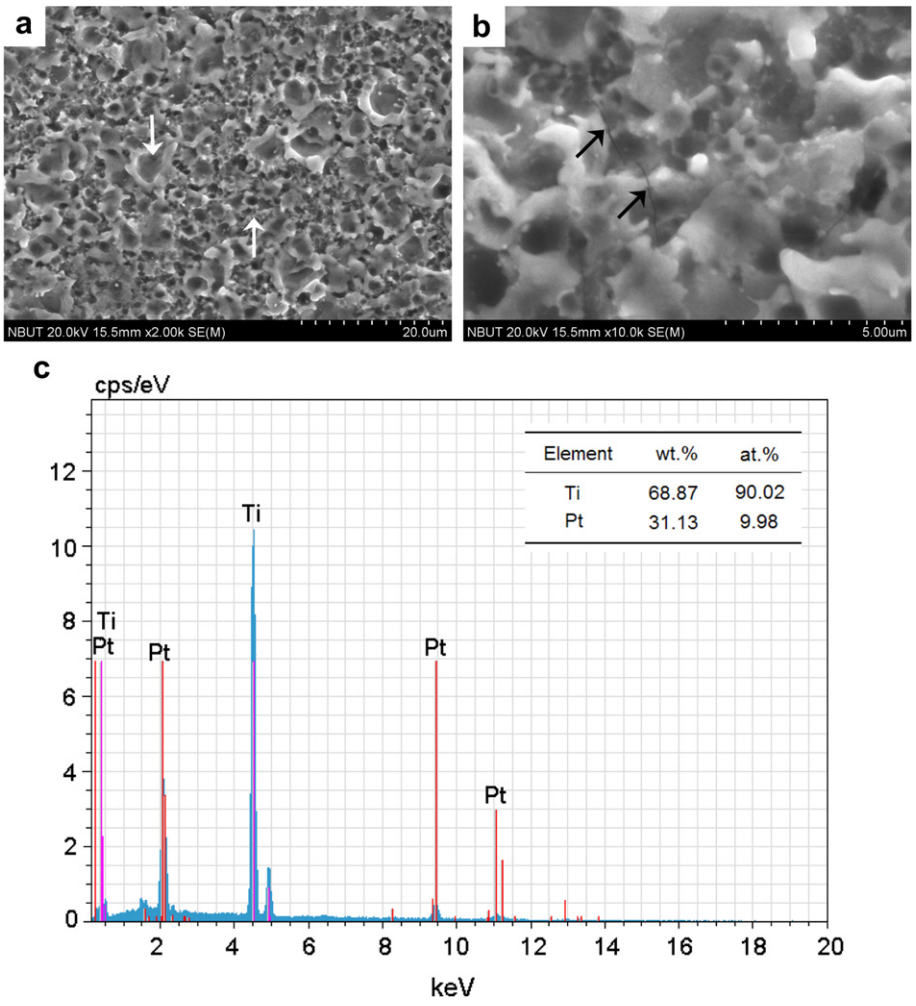

Fig. 4. (a, b) Top-view SEM micrographs and (c) corresponding EDX spectrum of $Pt_{arc\text{-}dep}Ti$ sample.

existence of micro-cracks herein should be attributed to the release of thermal-induced residual tensile stress, which derived from rapid solidification of molten droplets on the cold substrate. According to the corresponding EDX analysis, the surface of arc-deposited $Pt_{arc\text{-}dep}Ti$ is mainly composed of Ti and Pt with nominal compositional ratio of 90:10 (at. %). Due to the high compositional ratio between Ti and Pt, it is deduced that most of Pt sites were embedded in a form of islands surrounded by widespread Ti ensembles, which is also consistent with the surface XRD result mentioned above.

3.2. Electrochemical behavior and methanol oxidation on $Pt_{arc\text{-}dep}Ti$ electrode in alkaline media

Fig. 5 shows cyclic voltammetry (CV) curves for the bare Ti substrate and $Pt_{arc\text{-}dep}Ti$ electrodes in the 0.5 M KOH solution at a potential scan rate of 50 mV s^{-1}. Relative to the bland feature of Ti (Fig. 5a), the $Pt_{arc\text{-}dep}Ti$ electrode exhibits the typical electrochemical characteristics of Pt-related catalysts. As shown in Fig. 5b, three distinct electrochemical regions, including hydrogen adsorption/desorption, the formation and reduction of metallic oxide, and a non-Faradaic double-layer charging/discharging between them, can be clearly identified from the current response in the CV curve. In detail, the region in the potentials from −0.7 to −1.0 V is associated with the hydrogen (H_{upd}) adsorption/desorption, and is normally used to evaluate the electrochemically active surface area of Pt-based catalysts ($EASA_{Pt}$). Based upon the adsorption–desorption charge conversion factor of H_{upd} (210 μC cm^{-2}), the estimated $EASA_{Pt}$ was calculated to be 1.41 cm^2 for $Pt_{arc\text{-}dep}Ti$ electrode. It is puzzled that the $EASA_{Pt}$ is just comparable to the geometric area of $Pt_{arc\text{-}dep}Ti$ electrode (1.54 cm^2). Based upon the aforementioned microstructural analysis (XRD/EDX), it is deduced that only partial section of $Pt_{arc\text{-}dep}Ti$ surface was covered by Pt nano/micro-scaled spots (islands). Thus, the EASA of active Pt sites on $Pt_{arc\text{-}dep}Ti$ surface is reasonable in the present case. The broad plateau at ca. −0.1 V in the anodic scan and the peak at ca. −0.4 V in the cathodic scan correspond to the oxidation and reduction of Pt-related sites on the $Pt_{arc\text{-}dep}Ti$ surface, respectively. Relative to the CV curve of metallic Pt sheet (inset of Fig. 5b), it is interesting that a slightly sloping voltammogram is present for the $Pt_{arc\text{-}dep}Ti$. We assume that this sloping nature is possibly due to the intrinsic surface topography of $Pt_{arc\text{-}dep}Ti$ with scattered Pt islands on Ti surroundings. The partial presence of as-evolved Ti-oxides, which surrounds the nano/micro-scaled Pt spots, may increase the resistance of arc-deposited film. Moreover, a relative broad profile of double-layer charging/discharging should also be attributed to the existence of Ti-oxides in the island gaps, increasing the electrode capacitance. Of course, an underlying explanation should be explored in the future work.

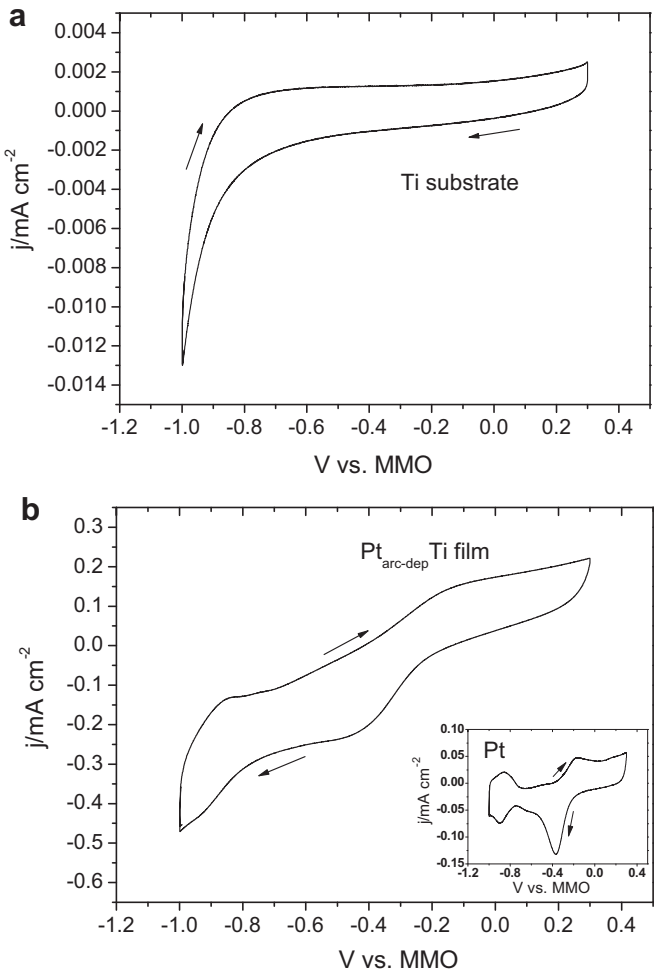

Fig. 5. CVs of (a) bare Ti and (b) $Pt_{arc\text{-}dep}Ti$ electrode in the 0.5 M KOH solution. Scan rate: 50 mV s^{-1}. Inset in (b) is the typical curve of Pt sheet electrode.

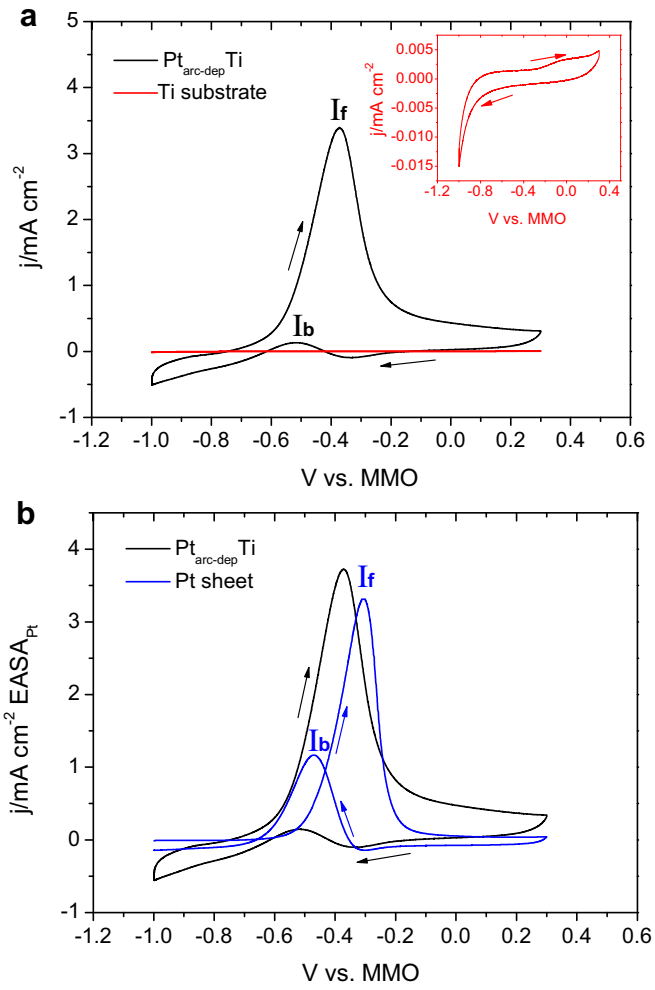

Fig. 6. (a) CVs of bare Ti and $Pt_{arc\text{-}dep}Ti$ electrode in the 0.5 M KOH + 1.0 M methanol solution (inset: the magnified curve from the bare Ti). (b) Comparison of $EASA_{Pt}$-normalized specific activity between $Pt_{arc\text{-}dep}Ti$ and Pt. Scan rate: 50 mV s^{-1}.

Fig. 6 shows the CVs of methanol oxidation at $Pt_{arc\text{-}dep}Ti$ electrode in the 0.5 M KOH + 1.0 M methanol solution. Before Pt arc-deposition, it displays no discernible methanol oxidation peaks at bare Ti electrode under the same test conditions (inset of Fig. 6a is the enlarged CV curve). On the contrary, two well-defined anodic oxidation peaks can be clearly observed in the CV curve when performing methanol electro-oxidation reaction at $Pt_{arc\text{-}dep}Ti$ electrode (Fig. 6a). Here, the onset potential (E_{op}) of methanol electro-oxidation at the $Pt_{arc\text{-}dep}Ti$ electrode is located at approximately −0.71 V. Moreover, the current density reaches its climax value of 3.38 mA cm^{-2} in the forward scan at peak potential (E_p) of −0.38 V. The decrease in the current density after −0.38 V is because the active sites on the surface of Pt and Pt-related intermetallic compounds are being oxidized and the oxidized active sites have no activity for methanol oxidation [32]. The current density in the reverse scan starts to increase at the potential of −0.35 V, which is consistent with the reduction of Pt oxide species on the $Pt_{arc\text{-}dep}Ti$ surface. Following the reduction of Pt oxide species, the active sites are recovered again so that the adsorbed intermediates may be further oxidized to generate oxidation current peak. Therefore, the oxidation current peak in the forward scan (I_f) corresponds to the oxidation of freshly chemisorbed species coming from methanol molecules, and is normally used to evaluate the catalytic activity of electrocatalysts [33,34]. Whereas, the current peak in the backward scan (I_b) is primarily associated with the oxidative removal of carbonaceous species which are not completely oxidized in the forward scan. And thus, the ratio of I_f/I_b is used to describe the tolerance to accumulation of carbonaceous species in some degree and is a rough indicator of the efficiency of catalysts [35,36]. In order to evaluate the actual activity enhancement of Pt atoms at $Pt_{arc\text{-}dep}Ti$ surface, the $EASA_{Pt}$-normalized activity for methanol oxidation was shown in Fig 6b. As compared with the Pt counterpart, it still exhibits a slightly higher current peak (3.72 mA cm^{-2}(Pt)) in the forward scan, which is ca. 1.12 times that of Pt (3.31 mA cm^{-2}(Pt)). However, it should be noted that the E_{op} and E_p of methanol oxidation at Pt sheet is located at −0.58 and −0.30V, exhibiting a positive potential shift of 130 and 80 mV as compared with those of $Pt_{arc\text{-}dep}Ti$, respectively. A more positive value of E_{op} and E_p indicates more sluggish oxidation kinetics at Pt electrode. Moreover, the ratio of I_f/I_b for methanol oxidation at Pt electrode is merely 2.85 while this ratio can reach to 26 at $Pt_{arc\text{-}dep}Ti$ surface. The larger I_f/I_b ratio also suggests the superior anti-poisoning performance of the $Pt_{arc\text{-}dep}Ti$ electrode.

Fig. 7 shows the correlation of methanol oxidation at $Pt_{arc\text{-}dep}Ti$ electrode as a function of methanol concentrations. CV curves shown in Fig. 7a were analyzed for the E_{op}, E_p, I_f, I_b and I_f/I_b ratio, respectively, and their values are shown in Table 1. It is clear that the E_{op} shifts negatively with increasing methanol concentrations.

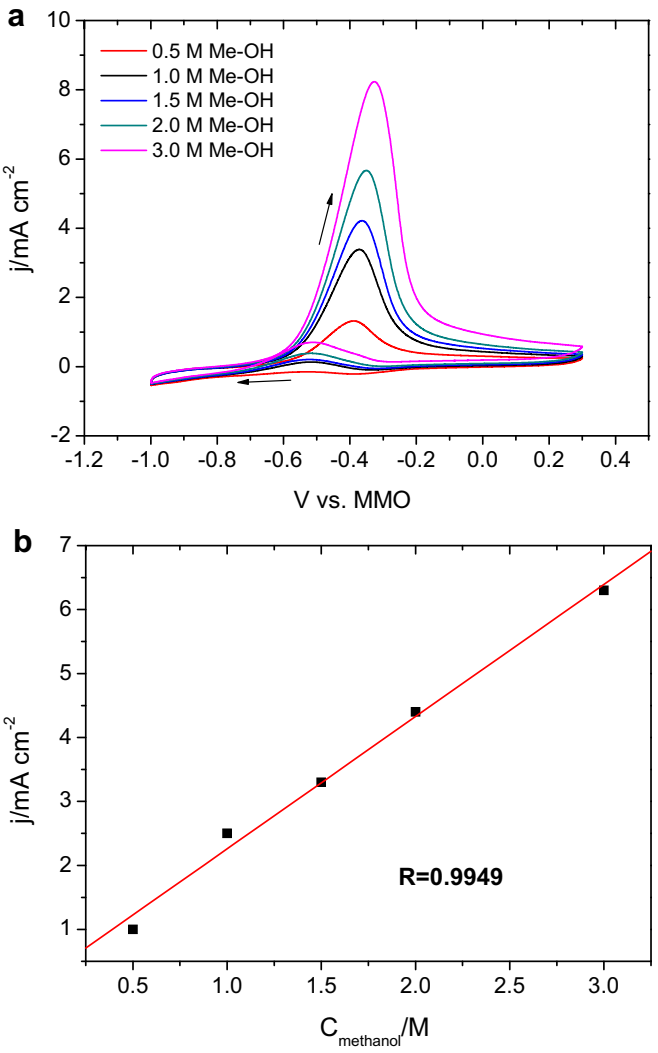

Fig. 7. (a) CVs of methanol oxidation at $Pt_{arc\text{-}dep}Ti$ electrode in 0.5 M KOH solution containing methanol with different concentrations. Scan rate: 50 mV s^{-1}. (b) The plots of forward peak current densities (I_f) versus methanol concentrations.

Obviously, the kinetics of methanol oxidation reaction can be promoted by the greater availability of alcohol molecules on the catalyst/electrolyte interface owing to the higher coverage level of reactant molecules on the $Pt_{arc\text{-}dep}Ti$ surface. In addition, the I_f increases significantly with increasing methanol concentrations from 0.5 to 3.0 M. Besides, the E_p slightly moves to high potentials with increasing methanol concentrations. As shown in Fig. 7b, the calibration plot further confirms a good linear relationship between oxidation current density and methanol concentration, indicating that the methanol electro-oxidation reaction is well-controlled by the methanol concentration at $Pt_{arc\text{-}dep}Ti$ surface.

Additionally, it is interesting to note that a higher I_f/I_b value is present for methanol electro-oxidation at $Pt_{arc\text{-}dep}Ti$ as compared with those reported in the previous work [37–39]. Generally, a high I_f/I_b ratio implies relatively complete oxidation of methanol to CO_2. In the case of Pt catalyst, the I_f/I_b ratio for methanol electro-oxidation is located at around 1. In some well-decorated or alloyed Pt-M bimetallic catalysts, the value of I_f/I_b may increase to a higher level due to the fact that reaction intermediates (i.e. CO-like species) can be efficiently removed in virtue of the introduction of adjacent oxophilic transition atoms so as to alleviate the catalyst poisoning (so-called bi-functional effect) [40,41].

Table 1
Cyclic voltammogram parameters of methanol electro-oxidation at $Pt_{arc\text{-}dep}Ti$ electrode in the 0.5 M KOH with different methanol concentrations.

$C_{methanol}$ /M	E_{op}/V	E_p/V	I_f/mA cm^{-2}	I_b/mA cm^{-2}	I_f/I_b
0.5	−0.68	−0.39	1.32	–	–
1.0	−0.71	−0.38	3.38	0.13	26
1.5	−0.74	−0.36	4.22	0.22	19
2.0	−0.75	−0.35	5.70	0.38	15
3.0	−0.77	−0.33	8.26	0.72	11

For example, Fu et al. [42] reported that the bimetallic core-shell Ni@Pt catalysts exhibit an enhanced I_f/I_b value for methanol oxidation in alkaline media and the values range from 4.38 to 2.61 by gradually modifying Pt/Ni atomic ratios, whereas the pure Pt catalyst has a much lower value of 2.54. Ou et al. [43] also claimed that Pt electrodeposited on TiC can significantly improve the ratio of I_f/I_b from ca. 2 to ca. 3.5 and ascribed this enhancement to the special anti-poisoning character of TiC. In the present work, it is noticed that the oxidation peak in the backward scan (I_b), which is considered to be proportional to the accumulation of carbonaceous species, is even hard to be distinguished in the methanol solution with a low concentration (i.e. 0.5 M) while only a single oxidation peak appears in the forward scan (I_f). In the 1.0 M methanol solution, the ratio of I_f/I_b can reach to ~26. With increasing methanol concentrations from 1.0 to 3.0 M, the ratios of I_f/I_b gradually reduce from ~26 to ~11. It agrees well with the fact that the higher the methanol concentration, the more severe the accumulation of carbonaceous species on the catalyst surface is. Fortunately, the ratio of I_f/I_b is still as high as ~11 at a higher methanol concentration of 3.0 M. This is a very significant and exciting result, as it indicates the better carbonaceous poisoning tolerance of $Pt_{arc\text{-}dep}Ti$ electrode in methanol electro-oxidation reaction.

Fig. 8 represents the plot of the forward peak current density of methanol oxidation at $Pt_{arc\text{-}dep}Ti$ electrode versus the CV cycle number in the 0.5 M KOH + 1.0 M methanol solution. It is clear that the peak current density increases gradually with the increase of cycle number over the first 50 cycles. Thereafter, the peak current density is found to be stable without any decrease. The decreasing trend in current densities with the number of cycles as observed on other platinized electrodes like Pt coated on glassy carbon (Pt-GC),

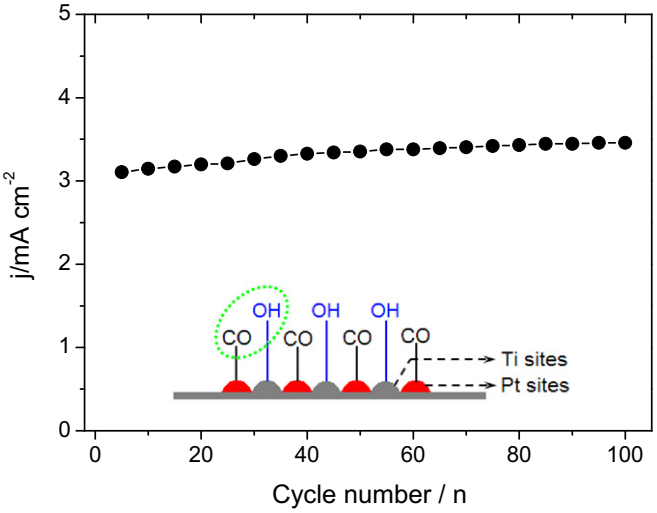

Fig. 8. The forward peak current densities of methanol oxidation at $Pt_{arc\text{-}dep}Ti$ electrode as a function of CV cycle number in the 0.5 M KOH + 1.0 M methanol solution. Scan rate: 50 mV s^{-1}. Inset: Scheme of anti-poisoning mechanism at $Pt_{arc\text{-}dep}Ti$ surface.

Pt/Ru-GC and Pt/Sn-GC [44] is not observed in the present case. It indicates that there exists no obvious poisoning of Pt active sites at $Pt_{arc\text{-}dep}Ti$ surface. Normally, the methanol oxidation reaction requires the co-adsorption of methanol and oxygen-containing species (i.e. OH_{ads}) on the surface of catalyst. Pt can adsorb and dehydrogenate methanol at relatively low potentials but it cannot adsorb OH at these potentials. It is therefore the objective of research on bimetallic catalysts to find a metal that can adsorb OH radical or any other oxygen-containing species at relatively lower potentials [45]. During the electro-oxidation reaction at $Pt_{arc\text{-}dep}Ti$ surface, methanol dehydrogenates mainly on Pt sites resulting in the formation of chemisorbed CO on Pt (Pt–CO). Based upon the intrinsic oxophilic character, the presence of surrounding Ti sites leads to the formation of Ti-OH functional groups at low over-potentials where CO is accumulated on Pt sites. The Pt sites will be regenerated by the bi-functional action of OH group present on neighboring Ti sites ($Pt{-}CO + Ti{-}OH \rightarrow Pt + Ti + CO_2 + H^+ + e^-$), and thus the poisoning can be eliminated simultaneously (inset of Fig. 8).

Chronoamperometric technique is another efficient method to evaluate the electrocatalytic activity and stability of catalysts. Fig. 9 shows the typical current density–time (i–t) response of methanol oxidation reaction at $Pt_{arc\text{-}dep}Ti$ surface. Compared to the current density obtained at $Pt_{arc\text{-}dep}Ti$ electrode, the chronoamperometric curve of the bare Ti even displays a flat profile and the as-evolved oxidation current density can be neglected, indicating that the bare Ti is inert toward methanol electro-oxidation (Fig. 9a). In order to further reveal the poisoning tolerance of Pt active sites at $Pt_{arc\text{-}dep}Ti$ surface, a comparison of $EASA_{Pt}$-normalized i–t curve between $Pt_{arc\text{-}dep}Ti$ and Pt sheet was also depicted (Fig. 9b). During continuous methanol oxidation at the catalyst surface, a slow decay of oxidation current density with time implies the formation of some Pt (and/or Ti) oxides/hydroxides and adsorbed intermediates if the kinetics of removal reaction could not keep pace with that of methanol oxidation. Nevertheless, the potentiostatic oxidation current density is obviously larger at $Pt_{arc\text{-}dep}Ti$ than that at Pt sheet over the test range. This indicates that the $Pt_{arc\text{-}dep}Ti$ is more efficient and poisoning tolerant compared to Pt in alkaline media, which is consistent well with the CV analysis mentioned above.

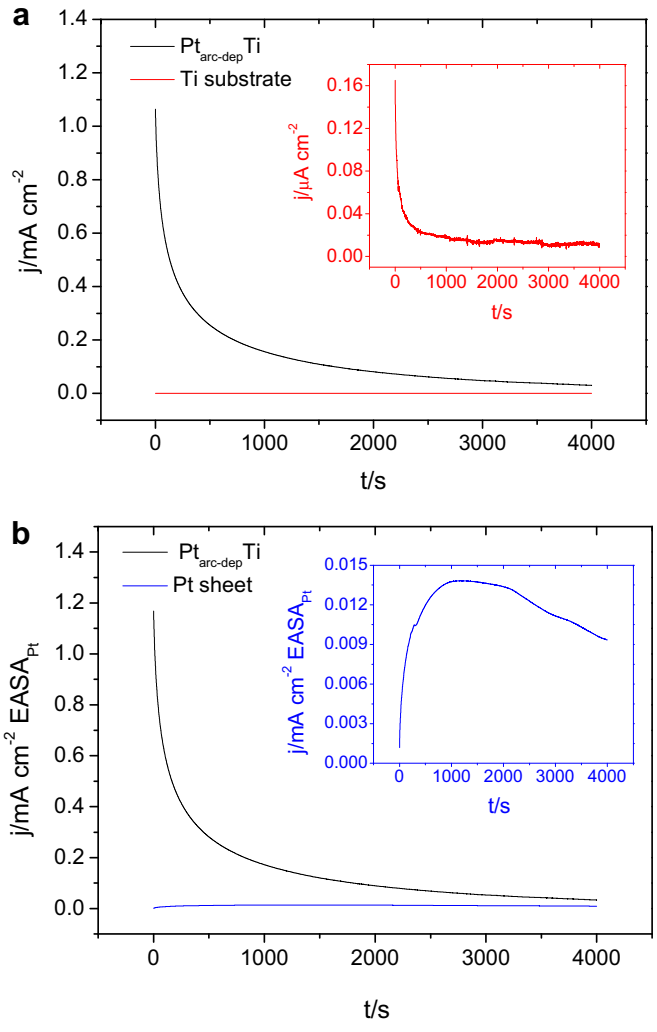

Fig. 9. (a) Chronoamperometric curves at −0.4 V for 4000 s at bare Ti and $Pt_{arc\text{-}dep}Ti$ electrode in the 0.5 M KOH + 1.0 M methanol solution (inset: the magnified curve from the bare Ti). (b) Comparison of $EASA_{Pt}$-normalized i–t relationship between $Pt_{arc\text{-}dep}Ti$ and Pt (inset: the magnified curve from the Pt sheet).

Generally, the activity enhancement could be explained by geometric (lattice mismatch, strain, defects and/or dislocations, etc) effects and/or electronic (d-band) effects [46,47]. Mehandru et al. [48] have reported that, bonding of Pt to Ti produces a dramatic decrease in density of states (DOS) near the Fermi level and an increase in the DOS near the d-band bottom. The equilibration of Fermi levels leads to electron flow from Pt to Ti rendering Pt slightly positive. This deficiency of electrons on Pt may create d-band vacancies which will eventually result in a decreased back donation to the CO bonding orbital. Similar electron deficiency and decrease in back donation have also been depicted when Pt is alloyed or adjacent with Ru, Fe, Co and Ni [49,50]. This will subsequently decrease the strength of Pt–CO bonding. Additionally, the slight positive charge on Pt may also enhance nucleophilic attack by water which in turn would help in the removal of adsorbed CO on Pt sites. It should also be pointed out that a decrease in CO desorption temperature has been reported when Pt is loaded onto a support such as W, Mo, TiN, WC and is also explained by the electron deficiency on Pt [51–54]. Furthermore, it is well-documented that electrocatalytic activity and anti-poisoning of Pt also depend on the crystallographic structure and strain state of Pt micro-crystallites deposited on the supports [55–58]. On the basis of these studies, it is reasonable to assume that the high methanol electro-oxidation activity especially the promising anti-poisoning performance of $Pt_{arc\text{-}dep}Ti$ electrode may originate from the following structural and chemical effects: (1) the adjacent Ti may alleviate CO poisoning effect on Pt owing to a similar bi-functional effect; (2) the bonding of Ti may change the electronic structure of Pt so as to enhance the catalytic activity of Pt toward methanol oxidation as well as the CO desorption; (3) the instantaneous high-energy arc-melt following by rapid solidification process may induce distortion of lattice, exposure of high-index facets as well as introduction of crystal defects to supply much more active sites. Of course, the in-depth reason should be explored relying on more sophisticated instruments in the future work.

4. Conclusions

Using the HEMAC technique, a novel $Pt_{arc\text{-}dep}Ti$ electrode was successfully fabricated. The microstructural characterization demonstrated that the $Pt_{arc\text{-}dep}Ti$ surface mainly comprises Ti, Pt, Pt_3Ti and $PtTi_3$. Moreover, a coarsening topographical feather can be observed, being composed of numerous craters/spots with sizes ranging from nano-scales to several microns. The $Pt_{arc\text{-}dep}Ti$ alleviates the CO poisoning effect with a higher ratio of the forward anodic peak current (I_f) to the reverse anodic peak current (I_b) for methanol electro-oxidation. The superior electrocatalytic

performance of $Pt_{arc\text{-}dep}Ti$ may be ascribed to this peculiar HEMAC process, which brings a series of favorable factors such as alloying effect, crystalline defects, and so forth. The HEMAC approach is generally facile to be implemented and thus an attractive choice for electrode functionalization, opening up enormous opportunities for platinum-related technological applications.

Acknowledgments

The authors acknowledge financial support by National Natural Science Foundation of China (51201113, 51171125), National Basic Research Program of China (973, 2012CB932800), the 51st China Postdoctoral Science Foundation (2012M510781), Program for New Century Excellent Talents in University (MOE) and Taiyuan University of Technology Talents Fund.

References

[1] M. Zhiani, B. Rezaei, J. Jalili, Int J Hydrogen Energy 35 (2010) 9298–9305.
[2] W.Q. Zhou, C.Y. Zhai, Y.K. Du, J.K. Xu, P. Yang, Int J Hydrogen Energy 34 (2009) 9316–9323.
[3] J.F. Whitacre, T. Valdez, S.R. Narayanan, J. Electrochem. Soc. 152 (2005) A1780–A1789.
[4] T. Shimizu, T. Momma, M. Mohamedi, T. Osaka, S. Sarangapani, J. Power Sources 137 (2004) 277–283.
[5] B. Beden, J.M. Leger, C. Lamy, in: J.O'M. Bockris, B.E. Conway, R.E. White (Eds.), Modern Aspects of Electrochemistry, vol. 22, Plenum Press, New York, 1992.
[6] L.X. Yang, W.Y. Yang, Q.Y. Cai, J. Phys. Chem. C 111 (2007) 16613–16617.
[7] A.V. Tripkovic, K.D. Popovic, J.D. Momcilovic, D.M. Draic, J. Electroanal. Chem. 418 (1996) 9–20.
[8] N.M. Markovic, T.J. Schmidt, B.N. Grgur, H.A. Gasteiger, R.J. Behm, P.N. Ross, J. Phys. Chem. B 103 (1999) 8568–8577.
[9] A. Verma, S. Basu, J. Power Sources 145 (2005) 282–285.
[10] J.R. Varcoe, R.C.T. Slade, Fuel Cells 5 (2005) 187–200.
[11] P. Gouérec, L. Poletto, J. Denizot, E. Sanchez-Cortezon, J.H. Miners, J. Power Sources 129 (2004) 193–204.
[12] M. Cifrain, K.V. Kordesch, J. Power Sources 127 (2004) 234–242.
[13] E. Antolini, J.C. Salgado, E.R. Gonzalez, J. Power Sources 160 (2006) 957–968.
[14] T.C. Deivaraj, W.X. Chen, J.Y. Lee, J. Mater. Chem. 13 (2003) 2555–2560.
[15] J.W. Guo, T.S. Zhao, J. Prabhuram, C.W. Wong, Electrochim. Acta 50 (2005) 1973–1983.
[16] H. Kim, N.P. Subramanian, B.N. Popov, J. Power Sources 138 (2004) 14–24.
[17] J.P. Wang, P. Holt-Hindle, D. MacDonald, D.F. Thomas, A.C. Chen, Electrochim. Acta 53 (2008) 6944–6952.
[18] N. Parkansky, I.I. Beilis, L. Rapoport, R.L. Boxman, S. Goldsmith, Y. Rosenberg, Surf. Coat. Technol. 105 (1998) 130–134.
[19] C.J. Chen, M.C. Wang, Y.M. Liu, D.S. Wang, R. Jin, J. Mater. Process. Technol. 198 (2008) 275–280.
[20] S. Frangini, A. Masci, A.D. Bartolomeo, Surf. Coat. Technol. 149 (2002) 279–286.
[21] J. Liu, R.J. Wang, Y.Y. Qian, Surf. Coat. Technol. 200 (2005) 2433–2437.
[22] Z. Chen, Y. Zhou, Surf. Coat. Technol. 201 (2006) 1503–1510.
[23] L. Tamašauskaitė-Tamašiūnaitė, A. Balčiūnaitė, A. Vaiciukevičienė, A. Selskis, V. Pakštas, J. Power Sources 208 (2012) 242–247.
[24] M.A.A. Rahim, H.B. Hassan, Thin Solid Films 517 (2009) 3362–3369.
[25] H.B. Hassan, J. Fuel Chem. Technol. 37 (2009) 346–354.
[26] Q.F. Yi, J.J. Zhang, A.C. Chen, X.P. Liu, G.R. Xu, Z.H. Zhou, J. Appl. Electrochem. 38 (2008) 695–701.
[27] Z.G. Shao, F.Y. Zhu, W.F. Lin, P.A. Christensen, H.M. Zhang, Phys. Chem. Chem. Phys. 8 (2006) 2720–2726.
[28] E.H. Yu, K. Scott, R.W. Reeve, L.X. Yang, R.G. Allen, Electrochim. Acta 49 (2004) 2443–2452.
[29] E.H. Yu, K. Scott, Electrochem. Commun. 6 (2004) 361–365.
[30] C.B. Tang, D.X. Liu, Z. Wang, Y. Gao, Appl. Surf. Sci. 257 (2011) 6364–6371.
[31] N. Parkansky, R.L. Boxman, S. Goldsmith, Surf. Coat. Technol. 61 (1993) 268–273.
[32] C.X. Xu, R.Y. Wang, M.W. Chen, Y. Zhang, Y. Ding, Phys. Chem. Chem. Phys. 12 (2010) 239–246.
[33] T.C. Deivaraj, J.Y. Lee, J. Power Sources 142 (2005) 43–49.
[34] Z.L. Liu, X.Y. Ling, X.D. Su, J.Y. Lee, J. Phys. Chem. B 108 (2004) 8234–8240.
[35] O.T.M. Musthafa, S. Sampath, Chem. Commun. (2008) 67–69.
[36] T. Maiyalagan, J. Solid State Electrochem. 13 (2009) 1561–1566.
[37] M.Y. Li, S.Z. Zhao, G.Y. Han, B.S. Yang, J. Power Sources 191 (2009) 351–356.
[38] D.S. Yuan, S.Z. Tan, Y.L. Liu, J.H. Zeng, F.P. Hu, X. Wang, P.K. Shen, Carbon 46 (2008) 531–536.
[39] Y.N. Wu, S.J. Liao, Z.X. Liang, L.J. Yang, R.F. Wang, J. Power Sources 194 (2009) 805–810.
[40] M. Watanabe, S. Motoo, J. Electroanal. Chem. 60 (1975) 267–273.
[41] T. Yajima, N. Wakabayashi, H. Uchida, M. Watanabe, Chem. Commun. (2003) 828–829.
[42] X.Z. Fu, Y. Liang, S.P. Chen, J.D. Lin, D.W. Liao, Catal. Commun. 10 (2009) 1893–1897.
[43] Y.W. Ou, X.L. Cui, X.Y. Zhang, Z.Y. Jiang, J. Power Sources 195 (2010) 1365–1369.
[44] S.M. Golabi, A. Nozad, Electroanalysis 15 (2003) 278–286.
[45] V.S. Bagotsky, Y.B. Vassiliev, O.A. Khazova, J. Electroanal. Chem. 81 (1977) 229–238.
[46] F. Maroun, F. Ozanam, O.M. Magnussen, R.J. Behm, Science 293 (2001) 1811–1814.
[47] P. Strasser, S. Koh, T. Anniyev, J. Greeley, K. More, C.F. Yu, Z.C. Liu, S. Kaya, D. Nordlund, H. Ogasawara, M.F. Toney, A. Nilsson, Nat. Chem. 2 (2010) 454–460.
[48] S.P. Mehandru, A.B. Anderson, P.N. Ross, J. Catal. 100 (1986) 210–218.
[49] L. Giorgi, A. Pozio, C. Bracchini, R. Giorgi, S. Turtuá, J. Appl. Electrochem. 31 (2001) 325–334.
[50] T. Toda, H. Igarashi, H. Uchida, M. Watanabe, J. Electrochem. Soc. 146 (1999) 3750–3756.
[51] A. Linsebigler, G.Q. Lu, J.T. Yates Jr., Surf. Sci. 294 (1993) 284–296.
[52] M.M.O. Thotiyl, T. Ravikumar, S. Sampath, J. Mater. Chem. 20 (2010) 10643–10651.
[53] D.J. Ham, Y.K. Kim, S.H. Han, J.S. Lee, Catal. Today 132 (2008) 117–122.
[54] M. Umeda, H. Ojima, M. Mohamedi, I. Uchida, J. Power Sources 136 (2004) 10–15.
[55] C. Lamy, J.M. Leger, J. Clavilier, R. Parsons, J. Electroanal. Chem. 150 (1983) 71–77.
[56] X.H. Xia, T. Iwasita, F. Ge, W. Vielstich, Electrochim. Acta 41 (1996) 711–718.
[57] S. Koh, P. Strasser, J. Am. Chem. Soc. 129 (2007) 12624–12625.
[58] P. Mani, R. Srivastava, P. Strasser, J. Phys. Chem. C 112 (2008) 2770–2778.